CHEMISTRY

废弃物中的稀土元素
Rare earth elements from waste

Bing Deng[1], Xin Wang[2], Duy Xuan Luong[1], Robert A. Carter[1], Zhe Wang[1], Mason B. Tomson[2], James M. Tour[1,3,4]*

稀土元素是电子和清洁技术中的关键材料。随着采矿用易得矿物的减少，从废物中回收稀土元素是循环经济的一种替代方法。
Rare earth elements (REEs) are critical materials in electronics and clean technologies. With the diminishing of easily accessible minerals for mining, the REE recovery from waste is an alternative toward a circular economy.
目前的稀土元素回收方法存在净化时间长、可萃取性低和废物流多的问题。
Present methods for REE recovery suffer from lengthy purifications, low extractability, and high wastewater streams.
在这里，我们报告了一种基于闪蒸焦耳热(FJH)的超快电热过程(~3000°C，~1s)，用于激活废物以提高REE提取能力。
Here, we report an ultrafast electrothermal process (~3000°C, ~1 s) based on flash Joule heating (FJH) for activating wastes to improve REE extractability.
FJH热降解或减少难溶REE物种，使其成为具有高热力学溶解度的组分，从而使浸出能力提高约2倍，并使用稀酸(例如0.1 M HCl)获得高回收率。
FJH thermally degrades or reduces the hard-to-dissolve REE species to components with high thermodynamic solubility, leading to ~2× increase in leachability and high recovery yields using diluted acid (e.g., 0.1 M HCl).
该活化策略适用于各种废物，包括粉煤灰、铝土矿残渣和电子废物。
The activation strategy is feasible for various wastes including coal fly ash, bauxite residue, and electronic waste.
快速FJH工艺节能，电能消耗低，为600 kWh/吨。
The rapid FJH process is energy-efficient with a low electrical energy consumption of 600 kWh ton^{-1}.
概述了该路线快速扩展的潜力。
The potential for this route to be rapidly scaled is outlined.

INTRODUCTION

稀土元素(REE)是现代电子、清洁能源和汽车工业的战略资源。
Rare earth elements (REEs) are strategic resources in modern electronics, clean energy, and automotive industries (*1*). Concentrated
稀土矿物的浓酸浸出，然后进行两相溶剂萃取，一直是稀土大规模生产的主要方案。
aqueous acid leaching of the REE minerals, followed by biphasic solvent extraction, has been the dominant scheme for REE mass
然而，资源和污染密集型生产的环境足迹很大，2015年的环境退化成本达到148亿美元，因此需要寻求可持续的解决方案。
production (*1*). However, the resource- and pollution-intensive production has a large environmental footprint, where the degrative environmental cost reached $14.8 billion in 2015, warranting a
随着易于获取的稀土矿物的减少，从工业废物中提取稀土元素已受到广泛关注。
search for a sustainable solution (*2*). As the easily accessible REE minerals diminish, the extraction of REE from industrial wastes has
适用的二次废物包括粉煤灰(CFA)；铝土矿残渣(BR；以前称为赤泥)，是铝土矿加工用于铝生产的结果；以及消费电子产品和电动汽车产生的电子废物(电子废物)。
gained much attention (*3*). The applicable secondary wastes include coal fly ash (CFA) (*4*–*9*); bauxite residue (BR; which was formerly called red mud) (*10*–*12*), which results from bauxite processing for aluminum production; and electronic waste (e-waste) (*13*–*15*) from
这些废物的再利用反过来又减少了其处置的环境负担。
consumer electronics and electric vehicles. The reuse of these wastes, in turn, reduces the environmental burden of their disposal (*8*).
然而，这些二次废物中的总稀土含量通常低于稀土矿物中的稀土含量，回收率仍然极低，这加剧了建立循环经济计划的努力。
However, the total REE contents in these secondary wastes are usually less than those in REE minerals, and the recycling yields are still extremely low, which exacerbate the quest to establish a circular economic program (*4*).

以CFA为例，它是煤炭燃烧的副产品，全球年产量约为7.5亿吨。
Taking CFA as an example, it is the by-product of coal combustion with an annual production rate of ~750 million tons worldwide
CFA的平均总稀土含量约为百万分之500(ppm)，这取决于原料煤的地质成因。
(*8*). CFA has an average total REE content of ~500 parts per million (ppm), which is variable based on the geological origin of the feed
然而，酸可提取的REE含量通常要小得多，并且高度依赖CFA进料。
coals (*4*, *9*). The acid-extractable REE content, however, is usually
例如，Taggart等人
much smaller and highly dependent on the CFA feeds. For example,
据报道，美国主要发电厂的REE HNO3可萃取性范围为1.6%至93.2%，中值约为30%，或7.4%至372 ppm，中值约为127 ppm。
Taggart *et al.* (*4*) reported the HNO_3 extractability of REE ranging from 1.6 to 93.2% with a median value of ~30% from major U.S. power plants, or 7.4 to 372 ppm with a median value of ~127 ppm (*4*). REE
CFA中的REE可萃取性取决于REE物种，如氧化物、磷酸盐(丘吉尔石、氟石、独居石等)、磷灰石、锆石和玻璃相。
extractability in CFA depends on the REE species, such as oxides, phosphates (churchite, xenotime, monazite, etc.), apatite, zircon, and glass phases (*7*).
大多数CFA资源的低REE可提取性归因于难溶REE物种的比例较大，如REE磷酸盐、锆石和玻璃相。
The low REE extractabilities in most CFA resources are attributed to the large ratios of hard-to-dissolve REE species such as REE phosphates, zircon, and glass phases (*7*).

优化酸浸工艺可以通过使用高浓度矿物酸在一定程度上提高萃取性，例如85°C至90°C下15 M HNO3的萃取率为70%，85°C下12M HCl的萃取率为35%至100%，具体取决于进料。
Optimizing acid leaching processes could, to some extent, improve the extractability by using highly concentrated mineral acids, such as 15 M HNO_3 at 85° to 90°C for an extractability of 70% (*4*) and 12 M HCl at 85°C for an extractability of 35 to 100%, depending
然而，使用浓酸不可避免地增加了提取成本和处理负担。
on the feeds (*16*). The use of concentrated acid, however, inevitably increases the cost of extraction and the disposal burden. Chemical
酸浸前CFA的化学或热预处理有助于实现高REE回收率。
or thermal pretreatment of the CFA before acid leaching contributes
例如，通过NaOH水热处理，然后进行酸浸，可实现88%的总稀土回收率。
to achieving high REE recovery (*17*, *18*). For example, a total REE recovery of 88% is achieved by the NaOH hydrothermal treatment
使用NaOH进行碱焙烧，回收率大于90%。
followed by acid leaching (*17*). Alkali roasting using NaOH leads to a recovery yield of >90% (*18*).
然而，这些预处理过程通常耗时且能耗高，这大大降低了利润率和激励。
However, those pretreatment processes are usually lengthy and energy-intensive, which greatly reduce the
因此，快速、节能的预处理是从废弃物中回收稀土元素的必要条件。
profit margin and incentive. Hence, a rapid and energy-efficient pretreatment is imperative for the REE recovery from waste products.

近年来，电加热作为一种超高速、高温、节能的材料合成和加工加热方式正在兴起。
Recently, electrical heating has been emerging as an ultrafast, high-temperature, and energy-efficient heating manner for materials
例如，高温冲击技术使用快速脉冲电流进行功能纳米材料的超快合成。
synthesis and processing. For example, the high-temperature shock technique uses rapid pulsed current for the ultrafast synthesis of
提出了一种基于连续电流输入的超高温烧结方法，用于陶瓷烧结和筛选，时间为秒。
functional nanomaterials (*19*–*22*). The ultrahigh-temperature sintering based on continuous current input is proposed for ceramic
我们的团队开发了闪蒸焦耳热(FJH)工艺，用于将含碳源转化为闪蒸石墨烯。
sintering and screening in seconds (*23*). Our group developed the flash Joule heating (FJH) process for conversion of carbon-containing
除了材料合成能力，FJH工艺已被证明是一种可持续管理富碳废物的有效技术，包括将塑料废物和橡胶废物转化为石墨烯。
sources into flash graphene (*24*). In addition to the materials synthesis capability (*25*), the FJH process has been demonstrated as an efficient technique for sustainable management of carbon-rich wastes (*26*), including the conversion of plastic waste (*27*) and rubber waste (*28*) to graphene.

在这里，我们报道了基于FJH的超快电热过程，以激活二次废物，仅使用弱酸(如0.1 M HCl)即可提高REE的酸萃取能力。
Here, we reported the ultrafast electrothermal process based on FJH to activate the secondary wastes to improve the acid extractability of REE simply using a mild acid such as 0.1 M HCl.
1秒内的脉冲电压使原料温度达到3000°C左右，导致CFA中难溶的稀土磷酸盐热分解为高可溶性稀土氧化物，稀土成分碳热还原为高活性稀土金属。
A pulsed voltage in 1 second brings the raw materials to a temperature of ~3000°C, leading to the thermal decomposition of the hard-to-dissolve REE phosphates in CFA into highly soluble REE oxides, and the carbothermic reduction of REE components to highly reactive REE metals.
与用更浓的酸直接浸出原料相比，活化工艺使F类CFA(CFA-F)和C类CFA(CFA-C)的REE回收率分别提高了约206%和约187%。
The activation process enables the increase in REE recovery yields to ~206% for class F-type CFA (CFA-F) and ~187% for class C-type CFA (CFA-C) compared to directly leaching the raw materials with more concentrated acids. The activation strategy is

[1]Department of Chemistry, Rice University, Houston, TX 77005, USA. [2]Department of Civil and Environmental Engineering, Rice University, Houston, TX 77005, USA. [3]Department of Materials Science and NanoEngineering, Rice University, Houston, TX 77005, USA. [4]Smalley-Curl Institute, NanoCarbon Center and the Welch Institute for Advanced Materials, Rice University, Houston, TX 77005, USA.
*Corresponding author. Email: tour@rice.edu

如CFA、BR和电子垃圾所示，活化策略适用于各种二次废物。
feasible for various secondary wastes, as demonstrated by CFA, BR,
快速FJH工艺具有可扩展性和高能效，电能消耗低至600千瓦时(kWh)吨1或12美
and e-waste. The rapid FJH process is scalable and highly energy-
元/吨，利润率大于10×。
efficient with a low electrical energy consumption of 600 kilowatt-hour
(kWh) ton^{-1} or \$12 ton^{-1}, enabling a profit percentage of >10×.
在所有REE中，其中五个(Y、Nd、Eu、Tb和Dy)是最关键的，这取决于它们对清洁能源设备的需求和
Among all REE, five of them (Y, Nd, Eu, Tb, and Dy) are most critical
供应风险。
based on their need for clean energy devices and their supply risk
FJH活化CFA、BR和电子废物中可提取临界REE的百分比比世界上一些最集中的矿石中的百分比高
(*29*). The percentages of extractable critical REE in the FJH-activated
出两到三倍，因此强调了这些当地资源的有用性，这些资源丰富，无需额外开采，被归类为有毒废物，
CFA, BR, and e-waste are two to three times higher than those in
难以储存。
some of the most concentrated ores in the world, thus underscoring
the usefulness of these local sources that are abundant, requiring no
additional mining, and categorized as toxic waste and problematic
to stockpile.

RESULTS

CFA中酸可萃取稀土含量

Acid-extractable REE content in CFA

按化学成分分为两种类型的CFA，CFA-F，SiO2、Al2O3和Fe2O3的总含量大于70%(wt%)，CFA-C，
There are two types of CFA categorized by the chemical composi-
CaO(7)的丰度较高。
tion, CFA-F, with the total content of SiO_2, Al_2O_3, and Fe_2O_3 >70
weight % (wt %), and CFA-C, with a higher abundance of CaO (*7*).
在这项工作中，CFA-F收集自阿巴拉契亚盆地(App)，CFA-C收集自美国的粉河流域(PRB)。
In this work, CFA-F is collected from the Appalachian Basin (App),
and CFA-C is collected from the Powder River Basin (PRB) (*4*),
如X射线衍射所示，CFA由初级非晶相(60-90%)组成，
both in the United States. CFA is composed of primary amorphous
剩余的结晶材料主要包括石英和莫来石
phases (60 to 90%) (*6*), and the remaining crystalline materials
include mainly quartz and mullite, as shown by the x-ray diffraction
(XRD)图(图1A)。除了Ca在CFA-C中富集外，通过X射线光电子能谱(XPS)
(XRD) patterns (Fig. 1A). In addition to the enrichment of Ca in
(图1B)和能量色散X射线能谱(图S1)进行的元素分析表明，CFA-F中的C含量较高，这可能是由于煤
CFA-C, elemental analyses by x-ray photoelectron spectroscopy
进料的不完全燃烧造成的。
(XPS) (Fig. 1B) and energy-dispersive x-ray spectroscopy (fig. S1)
show a high C content in CFA-F, which might be caused by the in-
通过热重分析(TGA)，CFA-F中的高C含量在约
complete combustion of coal feeds. The high C content in CFA-F is
700°C下的大重量损失也很明显(图S2)。
also evident by the large weight loss at ~700°C by thermal gravimet-
ric analysis (TGA) (fig. S2).

CFA中REE的总定量采用氢氟酸(HF)：HNO3消解法(详见材料和方法)。
The total quantification of REE in CFA was done by the hydro-
fluoric acid (HF):HNO_3 digestion method (see details in Materials
总REE含量，ctotal(CFA原始)，CFA-F为516±48 mg/kg，CFA-C
and Methods) (*4*). The total REE content, c_{total}(CFA Raw), is 516 ±
为418±71 mg/kg(图1C)。
48 mg kg^{-1} for CFA-F and 418 ± 71 mg kg^{-1} for CFA-C (Fig. 1C).
App的CFA的REE含量高于PRB，与之前的报告一致。
The CFA from App has a higher REE content than that from PRB,
使用1M HCl或15M HNO3测量CFA原料
consistent with a previous report (*4*). Acid-leachable REE contents
c0(CFA原料)中的酸浸出REE含量(详见材料和方法)。
from CFA raw materials, c_0(CFA Raw), were measured by using
1 M HCl or 15 M HNO_3 (see details in Materials and Methods)
对于CFA-F，HNO3-和HCl可提取的REE含量分别为144±32 mg/kg和160±50 mg/kg
(*4*, *9*). For CFA-F, the HNO_3- and HCl-extractable REE contents
(图1C)，对应的REE可提取性(Y0)分别约为28%和31%。
are 144 ± 32 mg kg^{-1} and 160 ± 50 mg kg^{-1} (Fig. 1C), respectively,
corresponding to the REE extractability (Y_0) of ~28 and ~31%, re-
对于CFA-C，HNO3-和HCl可提取的REE含量分别为246±71 mg/kg和231±81 mg/kg
spectively. For CFA-C, the HNO_3- and HCl-extractable REE contents
(图1C)，对应的REE可提取性分别为约59%和约55%。
are 246 ± 71 mg kg^{-1} and 231 ± 81 mg kg^{-1} (Fig. 1C), respectively,
corresponding to the REE extractability of ~59 and ~55%, respec-
得出的结论是，当酸浓度大于1 M时，对REE浸出能力的影响有限。因此，在以后的实验中，
tively. It is concluded that the acid concentration has limited effect
我们使用1M HCl浸出作为标准方案。
on the REE leachability once it is >1 M. Hence, in later experiments,
we used the 1 M HCl leaching as the standard protocol.

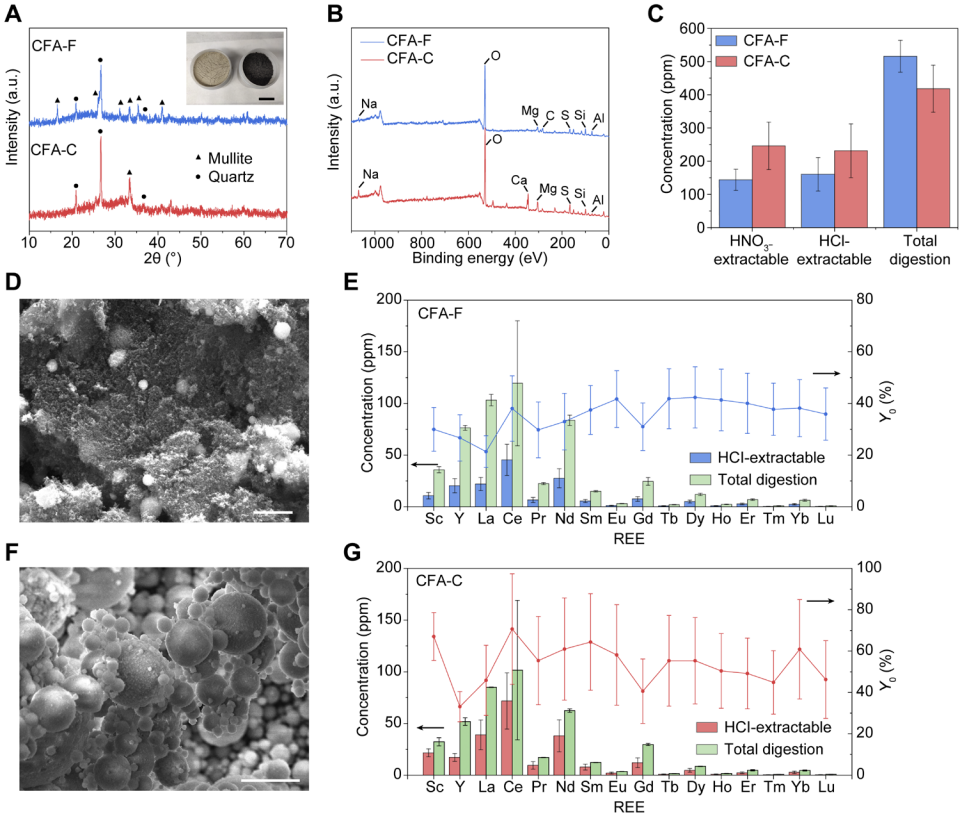

图1、CFA中的酸可萃取REE含量。(A)CFA-F和CFA-C的XRD图谱。插图：CFA-C(左)和CFA-F(右)的图片。比例尺，4厘米。任意单位。
Fig. 1. Acid-extractable REE content in CFA. (**A**) XRD patterns of CFA-F and CFA-C. Inset: Picture of CFA-C (left) and CFA-F (right). Scale bar, 4 cm. a.u., arbitrary units.
(B)CFA-F和CFA-C的XPS全谱。(C)通过HNO3浸出(15 M，85°C)、HCl浸出(1 M，85°C)和总量化，CFA-F和CFA-C中的总REE浓度。
(**B**) XPS full spectra of CFA-F and CFA-C. (**C**) Concentration of total REE in CFA-F and CFA-C by HNO_3 leaching (15 M, 85°C), HCl leaching (1 M, 85°C), and total quantification.
(D)CFA-F的SEM图像。比例尺，2 m。(E)HCl可萃取REE含量(1 M，85°C)和CFA-F中REE的总定量以及REE的回收率(Y0)。
(**D**) SEM image of CFA-F. Scale bar, 2 μm. (**E**) HCl-extractable REE contents (1 M, 85°C) and total quantification of REE in CFA-F and the recovery yield (Y_0) of REE. (**F**) SEM
(F)CFA-C的SEM图像。比例尺，5 μm。(G)HCl可萃取REE含量(1M，85°C)和CFA-C中REE的总定量以及REE的回收率(Y0)。(C)、(E)和(G)
image of CFA-C. Scale bar, 5 μm. (**G**) HCl-extractable REE contents (1 M, 85°C) and total quantification of REE in CFA-C and the recovery yield (Y_0) of REE. All error bars in
中的所有误差条表示SD，其中N=3。
(C), (E), and (G) represent the SD, where $N = 3$.

CFA-C中稀土元素的酸萃取率高于CFA-F。

The acid extractability of REE from CFA-C is higher than that 这与之前的一份报告一致，该报告将较高的可萃取性归因于CFA-C中易溶解

from CFA-F. This is consistent with a previous report (*7*), which 的稀土物种（如稀土氧化物）含量较高。

attributes the higher extractability to the higher content of easy-to- CFA-F的扫描电子显微镜

dissolve REE species like REE oxides in CFA-C. The morphology （SEM）形态图像如图1D所示，高碳含量可能会阻碍水酸对含稀土物种的可及性，导致单个稀土元素的可

image by scanning electron microscopy (SEM) of CFA-F is shown 萃取性较低，范围为21%~42%（图1E）。

in Fig. 1D, and the high carbon content could retard the accessibil-

ity of aqueous acids to REE-bearing species, leading to the low ex-

tractability ranging from 21 to 42% for individual REE (Fig. 1E). In 相比之下，CFA-C由细小的未覆盖的球形颗粒组成（图1F），这有利于酸浸过程，从而使单个REE的可提取

contrast, CFA-C is composed of fine, uncovered spheric particles 性相对较高，从33%到67%不等（图1G）。

(Fig. 1F), which benefits the acid leaching process, leading to a rela-

tively higher extractability ranging from 33 to 67% for individual

REE (Fig. 1G).

电热活化提高CFA中稀土元素的回收率

Improved recovery yield of REE from CFA by electrothermal activation

在FJH的电热活化过程中，CFA原料首先与炭黑（CB）混合，炭黑作为导电添加剂。

In our electrothermal activation process by FJH, CFA raw materials

were first mixed with carbon black (CB), which serves as the con- 将CFA和CB的混合物（约30 wt%CB）装入两个石墨电极之间的石英管中

ductive additive. The mixture of CFA and CB (~30 wt % CB) was （图2A和图S3）。

loaded inside a quartz tube between two graphite electrodes (Fig. 2A 通过调节连接到60 mF电容组的两个电极之间的压缩力，可以调节样品的电阻（R）

and fig. S3). The resistance (*R*) of the sample was tunable by adjusting （图S3）。

the compressive force between the two electrodes that were connected 通过电容器的高压放电使样品达到高温。

to a capacitance bank of 60 mF (fig. S3). The sample was brought to

a high temperature by high-voltage discharging of the capacitors. 详细的实验参数如表S1所示。

The detailed experimental parameters are shown in table S1. In a 典型的放电过程，FJH电压为120 V，R为1欧姆，放电时间为1s，记录通过样品的电流曲线，峰值电流

typical discharging process with FJH voltage of 120 V, *R* of 1 ohm, 约为120 A，随后电流平台约为7 A（图2B）。

and discharging time of 1 s, the current curve passing through the

sample was recorded with the peak current at ~120 A, followed by a 相应的实时温度曲线显示峰值温度高达3000 ° C左右，

current plateau at ~7 A (Fig. 2B). The corresponding real-time tem- 随后在1150 ° C左右稳定加热（图2C）。

perature curve exhibits a peak temperature up to ~3000°C, followed FJH期间样品的温度图显示，整个样品

by the stable heating at ~1150°C (Fig. 2C). The temperature map of 的温度分布均匀，没有明显的梯度（图S4），表明FJH具有均匀的加热能力。

the sample during the FJH shows that the temperature distribution

is uniform throughout the entire sample without an obvious gradi-

ent (fig. S4), demonstrating that the FJH has a homogeneous heat- 由于样品的电阻比石墨电极大得多，放电产生的热量主要施加在样品上（图S5）。

ing capability. Because the sample has a much larger resistance than

the graphite electrodes, the heat generated by discharging is mainly 因此，FJH装置具有良好的耐久性，即使可以达到

imposed onto the sample (fig. S5). Thus, the FJH setup has a good 如此高的温度。

durability even though such a high temperature can be achieved. FJH后获得的固体称为活化CFA（图S6）。

The obtained solid after the FJH is termed as activated CFA (fig. 通过1 M HCl浸出程序测量活化CFA c（活化CFA）中的可酸浸出REE含量。

S6). The acid-leachable REE content from the activated CFA, *c*(ac-

tivated CFA), was measured by the 1 M HCl leaching procedure. 计算活化CFA（Y）中稀土元素的回收率，并与CFA原料（Y0）的回收率进行比较（文本S1）。

The recovery yield of REE from the activated CFA (*Y*) was calculat-

ed and compared with that of the CFA raw materials (Y_0) (text S1). 施加一系列50至150 V的FJH电压（图2D）。

A series of FJH voltage ranging from 50 to 150 V were applied 在约120 V下，活化CFA-F中总REE（1 M HCl，85 ° C）的HCl可浸出含量提高至

(Fig. 2D). At ~120 V, the HCl-leachable content of total REE (1 M 329±14 mg/kg（图2D）。

HCl, 85°C) from the activated CFA-F is improved to 329 ± 14 mg 这相当于回收率约为64%，比CFA-F原料（0~31%）提高了约206%。

kg^{-1} (Fig. 2D). This corresponds to the recovery yield of Y ~ 64%,

representing an increase to ~206% over that of the CFA-F raw ma- 稀土元素的pH依赖浸出动力学

terials (Y_0 ~ 31%). The pH-dependent leaching dynamics of REE

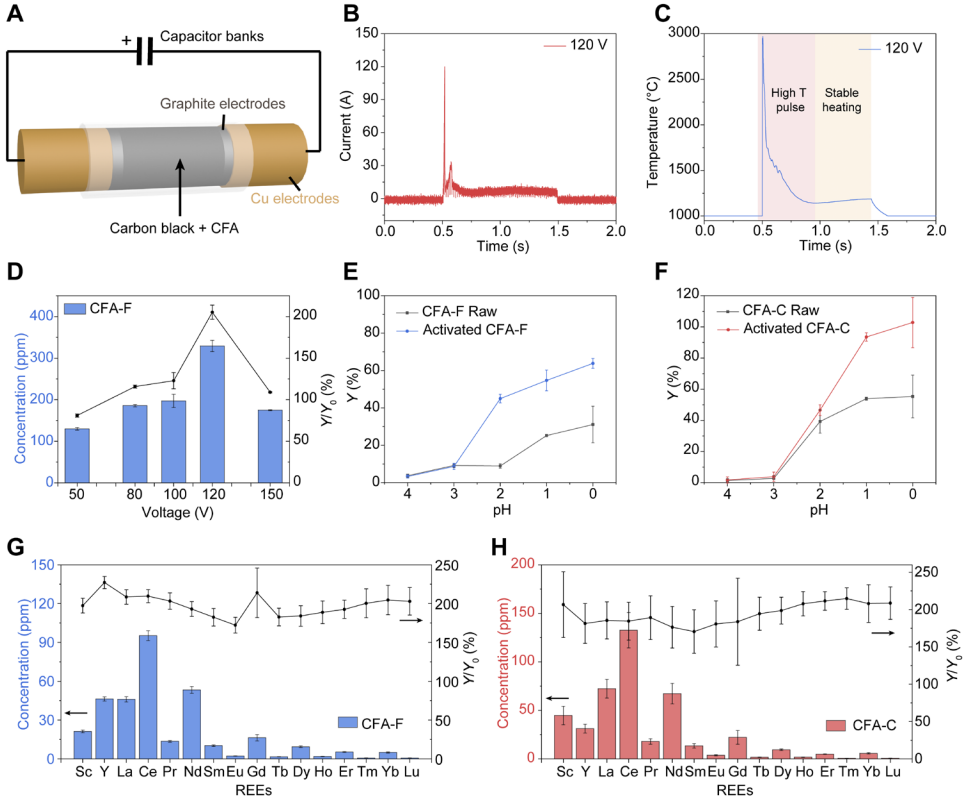

图2、通过电热活化提高CFA中稀土元素的回收率。（A）CFA FJH方案。（B）FJH条件为120 V和1s时的电流曲线。

Fig. 2. Improved recovery yield of REE from CFA by electrothermal activation. (**A**) Scheme of the FJH of CFA. (**B**) Current curve with the FJH condition of 120 V and 1 s. （C）在120 V和1s的FJH条件下进行实时温度测量。（D）活化CFA-F中HCl可浸出REE含量（1 M，85°C）、回收率增加（Y/Y0）与FJH电压之间的关系。

(**C**) Real-time temperature measurement with the FJH condition of 120 V and 1 s. (**D**) Relationship between HCl-leachable REE contents (1 M, 85°C) from activated CFA-F, （E）CFA-F原料和活化CFA-F的pH依赖REE浸出能力。（F）CFA-C原料和活化CFA-C中REE的pH依

increase in recovery yield (Y/Y_0), and the FJH voltages. (**E**) pH-dependent REE leachability from the CFA-F raw materials and activated CFA-F. (**F**) pH-dependent leachabil- 赖性浸出能力。（G）活化CFA-C中HCl可浸出的单个REE含量（1 M，85°C）和回收率的增加。

ity of REE from the CFA-C raw materials and activated CFA-C. (**G**) HCl-leachable individual REE contents (1 M, 85°C) from activated CFA-C and the increase in recovery yield. （H）活化CFA-F中HCl可浸出的单个REE含量（1M，85 ° C）和回收率的增加。 Y0表示盐酸浸出CFA原料的稀土回收率，Y表示盐酸浸出活化CFA的稀土回收率。

(**H**) HCl-leachable individual REE contents (1 M, 85°C) from activated CFA-F and the increase in recovery yield. Y_0 represents the REE recovery yield by HCl leaching the CFA （D）至（H）中的所有误差条表示SD，其中N=3。

raw materials, and *Y* represents the REE recovery yield by HCl leaching the activated CFA. All error bars in (D) to (H) represent the SD, where $N = 3$.

对CFA-F原料和活化CFA-F进行了研究(图2E)。
from CFA-F raw materials and activated CFA-F were investigated
通常，随着酸pH值的增加，产率降低。
(Fig. 2E). In general, the yield is reduced as the acid pH increases. The
活化CFA-F的REE回收率在pH 2(或0.01M HCl)下保持在约45%，大大高于相同浸出条件下(pH 2下
recovery yield of REE from the activated CFA-F remains $Y \sim 45\%$ at
为0～9%)，甚至在更高的酸浓度下(pH 0下为0～31%)。
pH 2 (or 0.01 M HCl), substantially higher than that of the CFA raw materials at the same leaching condition ($Y_0 \sim 9\%$ at pH 2), and even under a much higher acid concentration ($Y_0 \sim 31\%$ at pH 0). For
对于CFA-C，在优化的FJH条件下，使用HCl浸出程序(1M HCl，85°C)测量活化CFA-C中REE的酸浸出率
CFA-C, under the optimized FJH condition, the acid leachability of
约为Y 103%(图2F)，相当于CFA-C原料中REE的约187%(Y0～55%)。
REE from the activated CFA-C is measured to be $Y \sim 103\%$ using the HCl leaching procedure (1 M HCl, 85°C) (Fig. 2F), corresponding to
即使使用稀酸
~187% of that from the CFA-C raw materials ($Y_0 \sim 55\%$). Even using
(pH 1或0.1 M HCl)，活化CFA-C中稀土元素的回收率仍保持在94%左右，大大高于CFA-C原料的回收
a dilute acid (pH 1 or 0.1 M HCl), the recovery yield of REE from the
率(0～54%)。
activated CFA-C remains $Y \sim 94\%$, substantially higher than that of
这将使废水流更易于管理。
the CFA-C raw materials ($Y_0 \sim 54\%$). This would render far more manageable wastewater streams.

对于单个REE，采用FJH活化工艺，使用相同的浸出程序(1M HCl，85°C)，CFA-F(图2G)
For individual REE, with the FJH activation process, the acid
和CFA-C(图2H)的酸浸出率分别从约170%到约230%和约170%到约210%不等。
leachability is improved ranging from ~170 to ~230% for CFA-F (Fig. 2G) and from ~170 to ~210% for CFA-C (Fig. 2H) using the
使用稀酸浸出(0.1 M HCl，
same leaching procedure (1 M HCl, 85°C). Similar improvements
85°C)实现了类似的改进(图S7)。
were realized using a dilute acid leaching (0.1 M HCl, 85°C) (fig.
观察到不同REE之间存在一些偏差，这可能是由于CFA中REE的分布不均匀(图1、E和F)，以及
S7). Some deviations among the different REE are observed, which
REE之间的活化程度不同(稍后将详细讨论)。
could be attributed to the inhomogeneous distribution of REE in CFA (Fig. 1, E and F), as well as the different activation degree
作为对照，使用相同的消解方法
among REE (as will be discussed in detail later). As control, the REE
测量CB中的REE含量(图S8)。
content in CB was measured using the same digestion method (fig.
CB中的总REE含量约为5 mg/kg，相当于CFA中的1%。
S8). The total REE content in CB is ~5 mg kg^{-1}, corresponding to
因此，使用CB不会给我们的测量带来显著误差。
~1% of that in CFA. Hence, the use of CB will not induce notable
在实际应用中，CB可以用无烟煤或任何其他廉价的中等导电
error into our measurement. In practical applications, the CB could
碳源代替，但在产量计算中需要考虑该源中的REE含量。
be substituted with anthracite coal or any other inexpensive sources of mildly conductive carbon, but the REE content in that source needs to be considered in yield calculations.

稀土元素可萃取性提高的机理

Mechanism of the improved REE extractability

然后，我们研究了电热活化过程改善稀土浸出能力的机理。
We then investigated the mechanism of the improved REE leach-
CFA中稀土元素的形态和分布决
ability by the electrothermal activation process. The REE speciation
定了稀土元素的可提取性。
and distribution in CFA determine the REE extractability. REE
稀土磷酸盐，包括独居石和氙酸盐，是煤中稀土元素的主要反离子之一。
phosphate, including monazite and xenotime, is one of the primary
REE磷酸盐是相当稳定的组分，在约2000°C的空气
counterions of REE in coal (*7*, *30*). REE phosphates are rather stable
中不会发生熔融或热分解。
components, and no melting or thermal dissociation of them occurs
燃煤燃烧温度通常在1300°至1700°C之间。
up to ~2000°C in air (*31*, *32*). The coal-fire combustion temperature
因此，含有稀土元素的微量相，包
typically ranges from 1300° to 1700°C (*30*). As a result, the REE-
括独居石和氙时，在CFA中持续存在。
bearing trace phases, including monazite and xenotime, persist in
REE也可以通过扩散到在燃煤锅炉温度下形成的熔体(例如铝硅酸盐)
CFA (*33*, *34*). The REE could also be partitioned and encapsulated
中，被分割并封装到CFA的玻璃部分中。
into the glass fraction of CFA by diffusion into the melt (e.g., alumi-
难溶解的REE磷酸盐
nosilicates) formed at the coal boiler temperature (*35*). Those hard-
和玻璃相对REE提取有害，而CFA中的REE氧化物和碳酸盐相对容易通过酸浸提取。
to-dissolve REE phosphates and glass phases are detrimental for REE extraction (*7*), while REE oxides and carbonates in CFA are relatively easier to extract by acid leaching.

FJH工艺产生的约3000°C的高温，大大高于燃煤锅炉的温度，可热降解REE物种。
The high temperature of ~3000°C generated by the FJH process, which is substantially higher than the coal boiler temperature, could
在标准条件下，REE磷酸盐的热分解温度计算
thermally degrade the REE species. The thermal decomposition
为约2600°C至约2900°C(表S2)。
temperatures of REE phosphates are calculated to be between
实验上，磷
~2600° and ~2900°C under standard conditions (table S2). Experi-
酸钇(YPO_4)和磷酸镧($LaPO_4$)被用作稀土磷酸盐的代表。
mentally, yttrium phosphate (YPO_4) and lanthanum phosphate
如图3A所示，在
($LaPO_4$) were used as representatives for REE phosphates. As shown
YPO4前体FJH后，在产物中识别出Y2O3相。
in Fig. 3A, after FJH of the YPO_4 precursor, the Y_2O_3 phase is iden-
类似地，LaPO4在FJH工艺后热分解为Y2O3(图3B)。
tified in the product. Similarly, $LaPO_4$ is thermally decomposed to
虽然我们不试图确定FJH期间获得的所有新材料相，
Y_2O_3 after the FJH process (Fig. 3B). While we not seeking to identify
但REE氧化物的溶解度(log10Ksp为5至33)远高于REE磷酸盐
all new material phases accessed during FJH, the REE oxides have much higher solubility ($\log_{10}K_{sp}$ of 5 to 33) than REE phosphates
(27至24的log10 Ksp)(表S3)。
为了进一步深入了解REE磷酸盐和氧化物的溶解度，
($\log_{10}K_{sp}$ of −27 to −24) (table S3). To further provide insight into
我们计算了溶解曲线作为pH值的函数(图3C)。
the solubility of REE phosphates and oxides, we calculated the dis-
研究发现，LaPO4和YPO4只有在pH
solution curves as a function of pH (Fig. 3C). It is found that $LaPO_4$
值接近0时才表现出显著的溶解性，而氧化物对应物在pH值为6的低酸度下容易溶解。
and YPO_4 show notable solubility only when pH approaches 0, while the oxide counterparts readily dissolve at a low acidity with
这部分解释了观察到的pH依赖性REE浸出动力学，即活化CFA的REE浸出率高于使用稀酸的原
pH ~6. This partially explains the observed pH-dependent REE leach-
材料(图2、E和F)。
ing dynamics that higher REE leachabilities are achieved for the activated CFA than the raw materials using dilute acid (Fig. 2, E and F).

除稀土磷酸盐的热分解外，FJH所达到的超高温也可能引发稀土化合物的热还原。
In addition to the thermal decomposition of REE phosphates, the ultrahigh temperature achieved by FJH could also trigger the thermal
根据计算的Ellingham图(图3D)，REE氧化物的碳热还
reduction of REE compounds. According to the calculated Ellingham
原温度估计在约1900°C(Eu_2O_3)和约2500°C(Sc_2O_3)之间。
diagram (Fig. 3D), the carbothermic reduction temperatures of REE oxides are estimated to be between ~1900°C (for Eu_2O_3) and ~2500°C
120 V左右的FJH产生高达3000°C的温度(图2C)，这允许还原所有REE氧化物。
(for Sc_2O_3). The FJH at ~120 V generates a temperature up to ~3000°C
以Y2O3和La2O3
(Fig. 2C), which permits the reduction of all REE oxides. Y_2O_3 and
为代表，验证了FJH工艺对稀土氧化物的碳热还原。
La_2O_3 were used as representatives to verify the carbothermic re-
FJH后Y2O3的XPS精细光谱拟合显示
duction of REE oxides by the FJH process. The fitting of the XPS
出四个峰(图3E和表S4)。
fine spectrum of Y_2O_3 after FJH shows four peaks (Fig. 3E and table
将157.5和159.6 eV处的峰值分别指认为Y2O3中Y的3d5/2和3d3/2(图S9A)，以及
S4). The peaks at 157.5 and 159.6 eV are assigned to $3d_{5/2}$ and $3d_{3/2}$
156.4和158.5 eV处的峰值分别指认给Y(0)中Y的3d5/2和3d3/2。
of Y in Y_2O_3, respectively (fig. S9A) (*36*), and the peaks at 156.4 and 158.5 eV are assigned to $3d_{5/2}$ and $3d_{3/2}$ of Y in Y(0), respectively
XPS分析证明，Y2O3通过FJH过程还原为Y金属，而Y2O3的小比例可能来自表面氧化。
(*37*). The XPS analysis proved the reduction of Y_2O_3 to Y metal by the FJH process, while the small ratio of Y_2O_3 might be from the
类似地，La2O3前体(图S9B)和FJH后La2O3(图3F和表S4)的XPS精细
surface oxidation. Similarly, the fitting of XPS fine spectra of La_2O_3
光谱拟合验证了La2O3还原为La金属。
precursor (fig. S9B) and La_2O_3 after FJH (Fig. 3F and table S4) veri-
具有低氧化状态的还原REE物
fies the reduction of La_2O_3 to La metal (*38*, *39*). The reduced REE
种是高活性材料，即使与纯水也容易发生反应。
species with low oxidation state are highly active materials that
REE金属溶解反应的计算吉布斯自由能变
readily react with even pure water (*40*). The calculated Gibbs free
化(G)值比REE氧化物的吉布斯自由能变化(G)值负得多(图3G和表S3)，表明REE金属的热
energy change (ΔG) values for the REE metal dissolution reaction
力学溶解度比其氧化物对应物大得多。
are much more negative than those of REE oxides (Fig. 3G and table S3), demonstrating a much larger thermodynamic solubility of REE metals than for their oxide counterparts.

上述分析表明，REE磷酸盐的热分解所需的热活化温度>2600°C，REE氧化物的碳热还原所需的热活
化温度>2500°C，这也提供了对电压相关REE浸出能力的深入了解(图2D)。
The above analysis suggests that the required temperature for
the thermal activation is >2600°C for thermal decomposition of REE phosphates and >2500°C for carbothermic reduction of REE oxides, which also provides insight into the voltage-dependent REE
120 V的FJH电压对于达到>2000°C的温度至关重要(图S10)，而
leachability (Fig. 2D). An FJH voltage of ≥120 V is essential for
<100 V的电压对REE浸出性的影响有限。
achieving a temperature of >2000°C (fig. S10), while a voltage of
然而，FJH电压(150 V)
<100 V has limited effect on the REE leachability. Nevertheless, too
过高会导致超过3000°C的长期高温，进而导致FJH过程中REE的蒸发损失。
high of an FJH voltage, ≥150 V, leads to a prolonged high temperature of >3000°C, which could, in turn, result in the evaporative loss
FJH工艺观察到的不同REE的不同活化程度(图
of the REE during the FJH process. The observed different activa-
2、G和H)可归因于其不同的固有热力学性质，特别是REE磷酸盐的不同热分解温度(表S2)和REE氧
tion degree for different REE by the FJH process (Fig. 2, G and H)
化物的碳热还原温度(图3D)。
could be attributed to their different intrinsic thermodynamic properties, specifically the varied thermal decomposition temperature of REE phosphates (table S2) and carbothermic reduction temperature of REE oxides (Fig. 3D).

除了价态形成之外，REE分布还影响可萃取性，其中包裹在或分布在玻璃相中的REE很难溶解。
In addition to speciation, the REE distribution also affects the extractability, where the REEs encapsulated in or distributed through-
FJH允许超快加热和快速冷却
out the glass phases are hard to dissolve (*7*). The FJH permits an
(>10^4 K/s；图2C)，这将导致CFA中玻璃相的热应力和开裂，从而改善浸出性。
ultrafast heating and rapid cooling (>10^4 K s^{-1}; Fig. 2C), which would induce thermal stress and cracking of the glass phases in CFA, contributing to the improved leachability.

电热活化过程的一般性

Generality of the electrothermal activation process

电热活化工艺可推广到其他稀土回收废物，包括BR和电子废物。
The electrothermal activation process could be extended to other waste products for REE recovery, including BR (*10*–*12*) and e-waste
BR是拜耳法生产氧化铝的废料。
(*13*–*15*). BR is the waste product of the Bayer process for alumina
BR是最丰富的工业废物之一，
production. BR is one of the most abundant industrial wastes, with

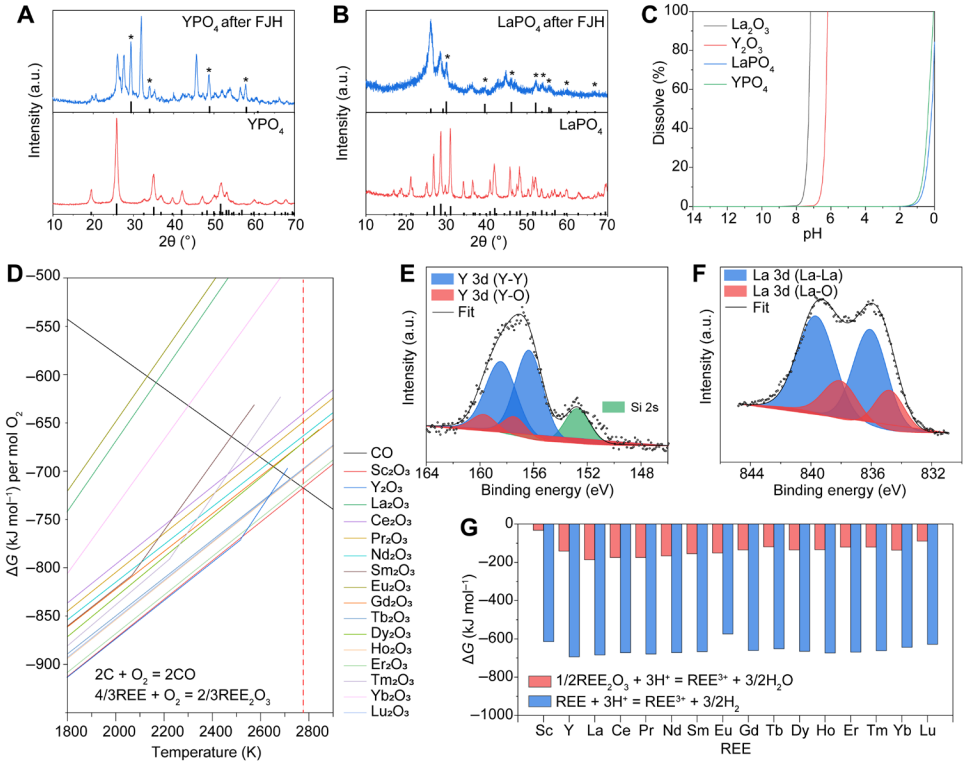

图3、电热活化提高稀土元素提取率的机理。

Fig. 3. Mechanism of the improved REE extractability by the electrothermal activation. (**A**) XRD patterns of YPO_4 (bottom) with reference PDF (YPO_4, #11-0254) and FJH(顶部)后的YPO4，参考PDF(Y2O3，#43-0661)。(B) LaPO4(底部)和参考PDF(LaPO4，#35-0731)的XRD图谱，以及FJH(顶部)之后的LaPO4和参考PDF(La2O3，#05-0602)的XRD图谱。 YPO_4 after FJH (top) with reference PDF (Y_2O_3, #43-0661). (**B**) XRD patterns of $LaPO_4$ (bottom) with reference PDF ($LaPO_4$, #35-0731) and $LaPO_4$ after FJH (top) with reference PDF (La_2O_3, #05-0602). The asterisks denote the diffraction peaks from La_2O_3. (**C**) Calculated dissolution curves of Y_2O_3, YPO_4, La_2O_3, and $LaPO_4$ with a mass of 1 g in 100-ml solution. Cl^- is used to balance the charge. (**D**) Ellingham diagram of carbon monoxide and REE oxides. The red dashed line denotes the temperature to reduce Sc_2O_3. (**E**) XPS fine spectrum of Y_2O_3 after FJH. The Si signal might be from the quartz tube during FJH. (**F**) XPS fine spectrum of La_2O_3 after FJH. (**G**) Gibbs free energy change of the REE oxide and REE metal dissolution reactions in acid.

(A)YPO4(底部)的XRD图，参考PDF(YPO4，#11-0254)和
星号表示La2O3的衍射峰。(C)计算质量为1 g的Y2O3、YPO4、La2O3和LaPO4在100 ml溶液中的溶解曲线。
Cl用于平衡电荷。
(D)一氧化碳和稀土氧化物的Ellingham图。
红色虚线表示降低Sc2O3的温度。(E)FJH后Y2O3的XPS精细光谱。
在FJH期间，Si信号可能来自石英管。
(F)FJH后La2O3的XPS精细光谱。
(G)稀土氧化物的吉布斯自由
能变化和稀土金属在酸中的溶解反应。

30亿吨已储存在废水池中，另外
3 billion tons already stored in waste ponds and an additional
每年生产1.5亿吨，但目前只有约3%被回收利用(41)。
150 million tons produced each year, yet just ~3% is currently recycled
BR含有大量的稀土元素，例如，希腊MYTILINEOS铝业的BR中的稀土元素总含量约为1000 ppm.
(*41*). BR contains a notable amount of REE, for example, a total
REE content of ~1000 ppm is found in BR from MYTILINEOS
BR是具有细粒度的干燥粉末(图S11)，其主要成分包
括Fe2O3、CaCO3、FeO(OH)和SiO2(图4A)。
"Aluminum of Greece" (*10*). The BR is a dried powder with fine
particle size (fig. S11) and has major components including Fe_2O_3,
BR中的稀土元素通过使用0.5 M HNO3的直
接浸出过程提取(详见材料和方法)。
$CaCO_3$, FeO(OH), and SiO_2 (Fig. 4A). The REE in BR was extracted
by a direct leaching process using 0.5 M HNO_3 (see details in Mate-
BR原料中的HNO3可萃取REE含量为428±9 mg/kg(图S12和
rials and Methods) (*42*). The HNO_3-extractable REE content from
图4B)。
BR raw materials is 428 ± 9 mg kg^{-1} (fig. S12 and Fig. 4B). Similar to
与CFA类似，电
热活化过程后BR的REE可萃取性也取决于FJH电压(图S12A)。
CFA, the REE extractability of the BR after the electrothermal acti-
vation process is also dependent on the FJH voltage (fig. S12A). At
在120 V的优化FJH电压下，HNO3可提取REE含量增加至757±30 mg/kg(图S12B)，相当于BR原料
the optimized FJH voltage of 120 V, the HNO_3-extractable REE
的Y/Y0～177%(图4B)。
content increased to 757 ± 30 mg kg^{-1} (fig. S12B), corresponding to
由于磷酸盐也是
Y/Y_0 ~ 177% of that from the BR raw materials (Fig. 4B). The mech-
BR(43)的主要反离子之一，FJH工艺改善BR中REE可萃取性的机理被认为与CFA相似(图3)。
anism of the improvement of REE extractability from BR by the
FJH process is presumed to be similar to that of CFA (Fig. 3), be-
cause phosphate is also one of the dominant counterions for BR (*43*).
我们还应用了FJH策略来激活电子垃圾。
We also applied the FJH strategy for activating e-waste. More
由于个人电子产品的快速升级，全球每年产生4000多万吨电子垃圾，其中回收率不到20%(44)。
than 40 million tons of e-waste are produced globally each year due
to the rapid upgrade of personal electronics, with <20% being recy-
稀土元素广泛应用于永磁体、电池和电容器等电子产品中。
cled (*44*). REEs are widely used in electronics in permanent mag-
反过来，与从矿石中开采稀土元素相
nets (*14*), batteries (*13*), and capacitors (*45*). In turn, the recovery of
比，从高品位电子废物中回收稀土元素具有经济可行性。
REE from high-grade e-waste has its economic feasibility compared
这项工作中使用的电子垃圾是印刷品
to REE mining from ores. The e-waste used in this work is a printed
废弃计算机的电路板(PCB)。
如图4C所示，电子垃圾
circuit board (PCB) from a discarded computer. As shown in
中丰富的金属包括铜和铝，它们主要用作导电。
Fig. 4C, the abundant metals in e-waste include Cu and Al, which
在85°C下，通过1M HCl浸出工艺提取PCB废
are mainly used as the interconnects. The REE in the PCB waste was
物中的REE(详见材料和方法)。
extracted by 1 M HCl leaching process at 85°C (see details in Mate-
来自电子废物原料的可酸浸REE含量为61±4 mg/kg(图S13)。
rials and Methods). The acid-leachable REE content is 61 ± 4 mg
在50 V的优化电压下进行活化
kg^{-1} from the e-waste raw materials (fig. S13). After the activation
处理后(图S13)，HCl可提取REE含量增加至94.6±0.2 mg/kg，相当于电子废物原料的Y/Y0～
process at an optimized voltage of 50 V (fig. S13), the HCl-extractable
156%(图4D和图S13)。
REE content is increased to 94.6 ± 0.2 mg kg^{-1}, corresponding to
Y/Y_0 ~ 156% of that from the e-waste raw materials (Fig. 4D and fig.
与CFA或BR不同，电子废物中的REE物种通常以易于溶解的REE金属或氧化物的形式存在。
S13). Different from CFA or BR, the REE species in e-waste are usu-
ally in the form of easy-to-dissolve REE metals or oxides (*45*). How-
然而，由于电子器件的层压结构，REE通常嵌入基体材料中，这可能会阻碍湿法冶金过程中的REE提取(图S14)。
ever, the REEs are usually embedded into the matrix materials
because of the laminated configuration of the electronics, which
could hinder the REE extraction by the hydrometallurgical process
FJH工艺可通过裂解基板来暴露REE物种，从而加快浸出速度和金属提取程度(图S14)。
(fig. S14). The FJH process could expose the REE species by crack-
ing the matrices, accelerating the leaching rate and extent of metal
extraction (fig. S14).

DISCUSSION

在所有可再生能源中，根据对清洁能源和供应风险的重要性，其中五种(Y、Nd、Eu、Tb和Dy)被认
Among all the REEs, five of them (Y, Nd, Eu, Tb, and Dy) are con-
为是最关键的。
sidered most critical based on the importance to clean energy and
活化CFA-F和CFA-C中HCl可萃取临界REE的百分比分别约为34%和26%
supply risk (*4*, *29*). The percentages of HCl-extractable critical REE
in activated CFA-F and CFA-C are ~34 and ~26%, respectively (fig.
(图S15，A和B)。
提取的临界REE百分比
S15, A and B). The percentages of the critical REE extracted from

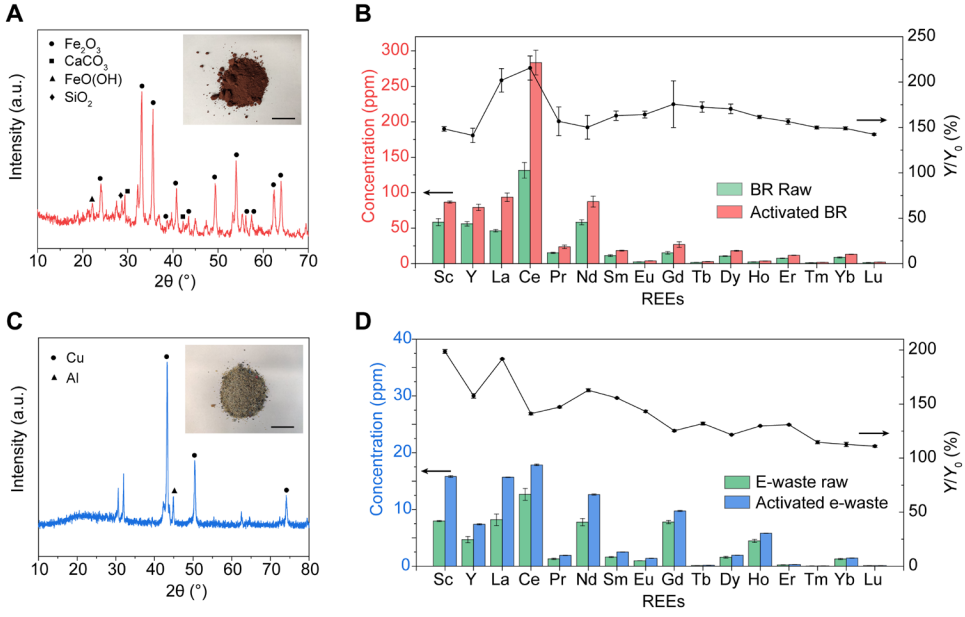

图4、从BR和电子废物中回收REE。（A）BR的XRD图谱。插图：BR的图片。比例尺，5厘米。（B）BR原料和120-V FJH活化BR的可酸浸单个REE含量（0.5 M HNO3）和回收率的增加（Y/Y0）。（C）电子废弃物的XRD图谱。插图：电子垃圾研磨成粉末的图片。比例尺，5厘米。（D）电子废物原料和50-V FJH活化电子废物中可酸浸出的REE含量（1M HCl）和回收率的增加。在（B）和（D）中，Y0表示原料酸浸的稀土回收率，Y表示活性物质酸浸的稀土回收率。（B）和（D）中的所有误差条表示SD，其中N=3。

Fig. 4. Recovery of REE from BR and e-waste. (**A**) XRD pattern of BR. Inset: Picture of BR. Scale bar, 5 cm. (**B**) Acid-leachable individual REE contents (0.5 M HNO_3) from BR raw materials and the 120-V FJH-activated BR and the increase in recovery yield (Y/Y_0). (**C**) XRD pattern of e-waste. Inset: Picture of e-waste ground to powders. Scale bar, 5 cm. (**D**) Acid leachable REE contents (1 M HCl) from e-waste raw materials and the 50-V FJH-activated e-waste and the increase in recovery yield. In (B) and (D), Y_0 represents the REE recovery yield by acid leaching the raw materials, and Y represents the REE recovery yield by acid leaching the activated materials. All error bars in (B) and (D) represent the SD, where $N = 3$.

CFA原材料和活化CFA几乎相同（图S15，A和B），表明FJH过程对不同REE没有区别性的活化性能。

the CFA raw materials and the activated CFA are almost identical (fig. S15, A and B), indicating that the FJH process shows no discriminative activation performance to different REE. In addition, the percentages of extractable critical REE in activated BR and e-waste are ~26 and ~29%, respectively (fig. S15, C and D). The critical REE percentages in these wastes are considerably higher than those in conventional ores (typically <15%) (*4*). For example, the world's largest REE deposit at Bayan Obo in China has a critical REE percentage of <10% (*46*). The higher percentage of critical REE in wastes compared to conventional minerals represents another major advantage of the recycling scheme.

此外，活性BR和电子废物中可萃取临界REE的百分比分别约为26%和29%（图S15，C和D）。这些废物中的临界REE百分比远远高于常规矿石中的REE百分比（通常<15%）。例如，中国白云鄂博的世界最大稀土矿床的临界稀土百分比小于10%。与传统矿物相比，废物中的关键REE百分比较高，这是回收计划的另一个主要优势。

REE恢复的FJH过程是可扩展的（文本S2和图S16和S17）。

The FJH process for REE recovery is scalable (text S2 and figs. S16 and S17). According to the theoretical analysis, to maintain a constant temperature when scaling up the sample mass per batch, we could increase the FJH voltage or the total capacitance of the capacitor bank (text S2). In our research laboratory, a production rate of >10 kg day^{-1} by the batch-by-batch process has already been realized (fig. S16). The FJH process could presumably be integrated into the continuous production manner for further automation (fig. S17). The major challenge for further scaling up the FJH process for REE recovery would be the design and construction of larger-scale equipment. This might be addressed by the application of the well-established high-voltage or even ultrahigh-voltage technologies in industry (*47*, *48*). In addition, the alternating current (AC) FJH (AC-FJH) could be introduced to complement the present direct current (DC) supply (*27*). The ongoing commercial scaling of the FJH process to tons per day paves the way for future REE recovery from large-scale waste products (text S2).

根据理论分析，为了在增加每批样品质量时保持恒温，我们可以增加FJH电压或电容器组的总电容（文本S2）。在我们的研究实验室中，已经实现了批量的生产速度>10kg/天。FJH工艺可能会集成到连续生产方式中，以实现进一步的自动化（图S17）。进一步扩大FJH稀土回收工艺的主要挑战是设计和建造大型设备。这可以通过在工业中应用成熟的高压甚至超高压技术来解决。此外，还可以引入交流（AC）FJH（AC-FJH）来补充目前的直流（DC）电源。FJH工艺目前的商业规模达到吨/天，为将来从大规模废物产品中回收稀土铺平了道路（文本S2）。

我们调查了经济效益，因为利润率通常是回收利用的支撑因素。

We investigated the economics because the profit margin is often the sustainer of recycling. Because of the direct sample heating feature, short duration, and rapid heating/cooling state, the FJH process is highly energy-efficient with a low electrical energy consumption of 600 kWh ton^{-1} or \$12 ton^{-1}, enabling a profit percentage of >10× compared to directly leaching the raw materials (text S3). For further refining, the removal of dissolved impurities, including mainly Al, Si, Fe, Ca, and Mg, in the REE-containing leachate and subsequent separation are needed (text S4). We observed that the content ratio of REE and impurity [c(REE)/c(Impurity)] in the leachate is improved with the FJH process in most cases (figs. S18 to S20), indicating that the FJH process would also be beneficial for the subsequent REE separation.

由于直接样品加热特性、持续时间短、加热/冷却速度快，FJH工艺高效节能，电能消耗量为600 kWh/吨或12美元/吨，与直接浸出原材料相比，利润率大于10倍（文本S3）。为了进一步精炼，需要去除含有稀土元素的渗滤液中的溶解杂质，主要包括Al、Si、Fe、Ca和Mg，然后进行分离（文本S4）。我们观察到，在大多数情况下，FJH工艺提高了渗滤液中稀土元素和杂质[c(REE)/c(杂质)]的含量比（图S18至S20），表明FJH工艺也有利于随后的REE分离。

由于独居石、（Ce，La，Y，Th）PO4和xenotime、YPO4是稀土生产的主要商业来源，因此拟定的活化策略也可用于稀土开采，以提高稀土矿石的浸出能力。

Because monazite, (Ce, La, Y, Th)PO_4, and xenotime, YPO_4, are the main commercial sources for REE production (*1*), the proposed activation strategy could also work for the REE mining to improve the leachability from REE ores. Commercially, alkaline digestion (70% NaOH, 140° to 150°C) is the main leaching technology for monazite (*49*) or acid baking (concentrated H_2SO_4, 200°C) for monazite and xenotime (*50*). The FJH strategy could be faster and less dependent on the use of concentrated bases and acids. Existing individual elemental separation technologies, such as solvent extraction and ion exchange (*51*), can be exploited to work with the REE mixtures obtained by FJH because these are often less contaminated than those generated through traditional mining methods (text S4).

在商业上，独居石的主要浸出技术是碱性消解（70%NaOH，140°至150°C），独居石和氣时的主要浸出技术是酸焙烧（200°C浓H2SO4）。FJH策略可以更快，更少地依赖于使用浓缩碱和酸。现有的个别元素分离技术，如溶剂萃取和离子交换，可用于FJH获得的REE混合物，因为这些混合物的污染程度通常比传统采矿方法产生的低（文本S4）。

材料和方法

MATERIALS AND METHODS

Materials

材料

所用化学品为La（NO3）3·6H2O（99 wt%，Fluka分析）、La2O3（99.9%，MilliporeSigma）、Y2O3（99.99%，MilliporeSigma）、YPO4（99.99%，Alfa-Aesar）、CB（Cabot，BP-2000）、H3PO4（85 wt%，Sigma-Aldrich）、HCl（37 wt%，99.999%，痕量金属等级，用于感应

The chemicals used are $La(NO_3)_3{\cdot}6H_2O$ (≥99 wt %, Fluka Analytical), La_2O_3 (99.9%, MilliporeSigma), Y_2O_3 (99.99%, MilliporeSigma), YPO_4 (99.99%, Alfa Aesar), CB (Cabot, BP-2000), H_3PO_4 (85 wt %, Sigma-Aldrich), HCl [37 wt %, ≥99.999% trace metal grade for inductively

耦合等离子体(ICP)分析，MilliporeSigma)、HNO3(67-70 wt%，用于ICP分析的痕量金属等级
coupled plasma (ICP) analysis, MilliporeSigma], HNO_3 (67 to 70 wt %,
，Fisher Chemical)、H2SO4(98 wt%，GR ACS等级(保证试剂符合美国化学学会标准)、
trace metal grade for ICP analysis, Fisher Chemical), H_2SO_4 [98 wt %,
MilliporeSigma)和HF(48 wt%，99.99%，用于ICP分析的痕量金属等级，MilliporeSigma)。
GR ACS grade (guaranteed reagent meeting American Chemical
Society standards), MilliporeSigma], and HF (48 wt %, ≥99.99%,
LaPO4是通过直接沉淀法
trace metal grade for ICP analysis, MilliporeSigma). $LaPO_4$ was syn-
合成的(52)。
thesized by direct precipitation (*52*). Concentrated H_3PO_4 was heated
将浓缩的H3PO4加热至150°C，缓慢添加
La(NO3)3·6H2O，以允许NOx气体的排放。
to a temperature of 150°C, and $La(NO_3)_3{\cdot}6H_2O$ was added slowly to
乳白色固体颗粒在30分钟内沉淀，然后使用砂芯漏斗
allow the emission of NO_x gas. Milky white solid particles precipi-
(F级)稀释并收集。
tated within 30 min, which were then diluted and collected by filtering
白色固体在烘箱(100°C)中干燥2小时。
using a sand core funnel (class F). The white solids were dried in an
CFA-F样品从App收集，CFA-C样品从PRB收集并提供给我们的实
oven (100°C) for 2 hours. The CFA-F samples were collected from
验室[见确认书(4)]。
App, and CFA-C samples were collected from PRB and provided to
BR是从希腊的MYTILINEOS S.A.收
our laboratory [see Acknowledgments (*4*)]. The BR was collected
集的，并提供给我们的实验室(见确认)。
from MYTILINEOS S.A. in Greece and provided to our laboratory
PCB废料来自一台废弃的计算机。
(see Acknowledgments). The PCB waste was from a discarded
PCB被切成小块，然后用锤式研磨机(Dade，DF-15)研磨成粉末。
computer. The PCB was cut into small pieces and then ground into
powders using a hammer grinder (Dade, DF-15).

FJH系统和流程

FJH system and process

FJH系统的电气图如图S3A所示。
The electrical diagram of the FJH system is shown in fig. S3A. The
FJH系统的图片如图S3B所示。 补充材料中列出了系统各电气
picture of the FJH system is shown in fig. S3B. The description of
部件的说明。
each electrical component of the system is listed in the Supplemen-
在典型实验中，使用球磨机(MSE Supplies，PWV1-0.4L)将二次废物(CFA
tary Materials. In a typical experiment, the secondary wastes (CFA,
、BR或电子废物)与CB以2:1的质量比混合。
BR, or e-waste) were mixed with CB with a mass ratio of 2:1 by us-
CB用作导电添加剂。
ing a ball miller (MSE Supplies, PWV1-0.4L). The CB served as the
将200 mg混合物(133 mg废物和67 mg CB)添加到石英管中
conductive additive. The 200-mg mixture (133 mg of waste and
(内径8 mm，外径12 mm)。
67 mg of CB) was added into a quartz tube (inner diameter of 8 mm
通过压缩两个电极来控制电阻。
and outer diameter of 12 mm). The resistance was controlled by
将样品装入夹具(图S3C)，并将电极连接到电容
compressing the two electrodes. The samples were loaded into the
器组。
jig (fig. S3C), and the electrodes were connected to the capacitor
总电容为60 mF的电容器组由直流电源充电。
bank. The capacitor bank with a total capacitance of 60 mF was
采用可编程毫秒级继电器控制放电时间。
charged by a DC supply. A relay with programmable milliseconds-
表S1总结了详细的实
level relay was used to control the discharging time. The detailed
验参数。 FJH后，样品迅速冷却至
experimental parameters are summarized in table S1. After the FJH,
室温。 为了将工艺放大到
the samples were rapidly cooled to room temperature. For the scal-
克级，构建并使用了总电容为0.624 F的更大FJH系统(图S3D)。
ing up of the process to the gram scale, a larger FJH system with a
使用较大的石
total capacitance of 0.624 F was built and used (fig. S3D). A larger
英管(内径16 mm，外径20 mm)和较大的反应夹具(图S3E)。
quartz tube (inner diameter of 16 mm and outer diameter of 20 mm)
安全警告：如果操作不当，有触电
and a larger reaction jig were used (fig. S3E). Safety caution: There
的风险。 FJH过程中，应佩戴
is a risk of electrical shock without proper operation. Safety glass
安全眼镜，以保护眼睛免受强光照射。
should be worn to protect the eyes from the bright light emission
应遵守单手规则，并应使用延伸至肘部的厚橡胶手套。
during the FJH process. The "one hand rule" should be obeyed, and
更多安全
thick rubber gloves extending to the elbows should be used. More
实施如图S3所示。
safety implementations were shown in fig. S3.

样品消解、浸出和ICP-MS/ICP-OES测量

Sample digestion, leaching, and ICP-MS/ICP-OES measurement

对于CFA样品，进行了酸可萃取REE含量测量，包括HNO3和HCl，以及总REE定量。
For the CFA samples, acid-extractable REE content measurement,
including HNO_3 and HCl, and total REE quantification were con-
对于HNO3浸出，约50 mg样品(CFA原料)在85°C的10 ml浓HNO3(15 M)中
ducted (*4*). For HNO_3 leaching, ~50-mg samples (CFA raw materi-
消解4小时。
als) were digested in 10-ml concentrated HNO_3 (15 M) at 85°C for
使用砂芯漏斗(F级)过滤样品，并使用超纯水稀释，以进行ICP质谱(MS)测量。
4 hours. The sample was filtered using a sand core funnel (class F)
and diluted using ultrapure water for ICP mass spectrometry (MS)
对于HCl浸出，约50 mg样品(CFA原料或FJH活化的CFA)在约10 ml HCl
measurement. For HCl leaching, ~50-mg samples (CFA raw mate-
(1 M)中于85°C下消解4小时。
rials or the activated CFA by FJH) were digested in ~10-ml HCl (1 M)
消解后，使用砂芯漏斗(F级)过滤样品，并使用超纯水稀释至约20
at 85°C for 4 hours. After digestion, the sample was filtered using a
ml，以进行ICP-MS测量。
sand core funnel (class F) and diluted to ~20 ml using ultrapure
使用0.1、0.01、0.001和0.0001 M研究了pH依赖
water for ICP-MS measurement. The pH-dependent leaching dy-
性浸出动力学
namics were investigated by using 0.1, 0.01, 0.001, and 0.0001 M
分别以pH值为1至4的HCl作为浸出剂。 样品(约50 mg；CFA原
HCl at pH 1 to 4, respectively, as the leaching agents. Samples (~50 mg;
料或FJH活化的CFA)在约10 ml的HCl中于85°C下消解4小时。
CFA raw materials or the activated CFA by FJH) were digested
消解后，使用砂芯漏斗(F级)过滤样品，
in ~10 ml of HCl at 85°C for 4 hours. After digestion, the sample
并使用HCl(2 wt%)稀释至约20 ml，以进行ICP-MS测量。
was filtered using a sand core funnel (class F) and diluted to ~20 ml
对于总REE定量，CFA原料(约
using HCl (2 wt %) for ICP-MS measurement. For total REE quan-
30 mg)在95°C下在浓缩HF(48 wt%，2 ml)和浓缩HNO3(15 M，2 ml)的混合物中消解过夜。
tification, CFA raw materials (~30 mg) were digested overnight at
95°C in a mixture of concentrated HF (48 wt %, 2 ml) and concen-
然后在100°C的烘箱中干燥样品，并在95°C的温度下，在浓
trated HNO_3 (15 M, 2 ml). The sample was then dried in an oven at
HNO3(15 M，1 ml)、H2O2(30-32%，1 ml)和超纯水(5 ml，高效液相色谱级)的混合
100°C and redigested overnight at 95°C in a mixture of concentrat-
物中重新消解过夜。
ed HNO_3 (15 M, 1 ml), H_2O_2 (30 to 32%, 1 ml), and ultrapure water
再消解后，溶
(5 ml, high-performance liquid chromatography grade). After the
解所有固体，并使用超纯水将样品稀释至50 ml，以进行ICP-MS测量。
redigestion, all the solids were dissolved, and the sample was diluted
to 50 ml using ultrapure water for ICP-MS measurement.
对于BR样品，测量了HNO3可萃取REE含量。
For the BR samples, HNO_3-extractable REE contents were mea-
样品(约50 mg；BR原料或FJH活化的BR)在室温下用HNO3(0.5 M)消解
sured. Samples (~50 mg; BR raw materials or the activated BR by
FJH) were digested using HNO_3 (0.5 M) at room temperature for
24小时。 使用砂芯漏斗(F级)过滤样品，以进行ICP-MS测量。
24 hours. The sample was filtered using a sand core funnel (class F)
for ICP-MS measurement.
对于电子废物样品，测量了HCl可提取的REE含量。
For the e-waste samples, HCl-extractable REE contents were
样品(约50 mg；电子废物原料或FJH活化的电子废物)在85°C下用10 ml HCl
measured. Samples (~50 mg; e-waste raw materials or the activated
(1 M)消解4小时。
e-waste by FJH) were digested using 10 ml of HCl (1 M) at 85°C for
然后使用砂芯漏斗过滤样品，并使用超纯水稀释至20 ml，以进行ICP-MS测量。
4 hours. The sample was then filtered using a sand core funnel and
diluted to 20 ml using ultrapure water for ICP-MS measurement.
对于CB作为对照，测量了HCl可提取的REE含量。
For the CB as control, HCl-extractable REE contents were mea-
使用10 ml HCl(1 M)在85°C下消解样品(约50 mg)，持续4小时。
sured. Samples (~50 mg) were digested using 10 ml of HCl (1 M) at
然后使用砂芯漏斗过滤样品，并使用超纯水稀释至20 ml，以进行ICP-MS测量。
85°C for 4 hours. The sample was then filtered using a sand core
funnel and diluted to 20 ml using ultrapure water for ICP-MS mea-
surement.
ICP-MS测量使用Perkinlemer Nexion 300 ICP-MS系统进行。
The ICP-MS measurement was conducted using a PerkinElmer
在测量中，主要的REE干扰是较轻元素的氧化物。
Nexion 300 ICP-MS system. In the measurement, the primary REE
为了避免引入显著误差，使用
interferences were oxides of lighter elements. To avoid the intro-
156:140(CeO/Ce)的质量比监测氧化物的形成，该质量比保持在3%以下。
duction of notable error, the formation of oxides was monitored
using a mass ratio of 156:140 (CeO/Ce), which was kept below 3%.
稀土元素的检测限为0.5至5万亿分之一(ppt)。
The detection limits for REE are in the level of 0.5 to 5 parts per
使用REE混合物标准(MilliporeSigma；用于ICP的周期表混合物3；16种元素；每
trillion (ppt). The REE mixture standard was used (MilliporeSigma;
种10 mg l1；Sc，Y，La，Ce，Pr，Nd，Sm，Eu，Gd，Tb，Dy，Ho，Er，Tm，Yb和Lu在5 wt%硝酸
periodic table mix 3 for ICP; 16 elements; 10 mg liter each; Sc,
中)。
Y, La, Ce, Pr, Nd, Sm, Eu, Gd, Tb, Dy, Ho, Er, Tm, Yb, and Lu in
在我们的分析中，这些标准的浓度范围为十亿分之一到1000分之一。
5 wt % nitric acid). In our analyses, the standards were in the con-
将所有分析样品仔细稀释至浓度
centration range of 1 to 1000 parts per billion. All the analyzed sam-
范围，该浓度范围至少比定量检测限高两个数量级。
ples were carefully diluted into the concentration range, which is at
least two orders of magnitude higher than the detection limit of
对所有样品进行三次测量，以得出SDs。
quantification. All the samples were measured three times to afford
the SDs.
还使用ICP-MS测量了浸出液中的杂质，包括铝、硅、铁、镁、锌、钴、镍、铬和铜。
The impurities, including Al, Si, Fe, Mg, Zn, Co, Ni, Cr, and Cu,
使用混合物标准(
in the leachates were also measured using the ICP-MS. The mixture
MilliporeSigma，用于ICP的周期表混合物1；33种元素；每种元素10 mg l；Al，As，Ba，Be，Bi，B
standard was used (MilliporeSigma, periodic table mix 1 for ICP; 33
、Ca，Cd，Cs，Cr，Co，Cu，Ga，In，Fe，Pb，Li，mg，Mn，Ni，P，K，Rb，Se，Si，Ag，Na，Sr，S
elements; 10 mg liter each; Al, As, Ba, Be, Bi, B, Ca, Cd, Cs, Cr, Co,
、Te，Tl，V和Zn，在10 wt%含HF痕量硝酸中)。
Cu, Ga, In, Fe, Pb, Li, Mg, Mn, Ni, P, K, Rb, Se, Si, Ag, Na, Sr, S, Te,
由于氩的一次
Tl, V, and Zn in 10 wt % nitric acid containing HF traces). ICP-MS
同位素为m/z(质量/电荷比)=40，因此很难使用ICP-MS来定义Ca。因此，ICP光发射光谱法
is difficult to be used to define Ca due to the primary isotope of ar-
(ICP-OES)被用于量化钙。
gon, which is at *m/z* (mass/charge ratio) = 40. Hence, ICP optical
emission spectrometry (ICP-OES) was used to quantify Ca. The
使用Perkinlemer Optima 8300 ICP-OES进行ICP-OES测量。
ICP-OES measurement was conducted using a PerkinElmer Opti-
ma 8300 ICP-OES.

表征

Characterization

使用FEI Quanta 400 ESEM场发射显微镜在10 kV下获得SEM图像。
SEM images were obtained using a FEI Quanta 400 ESEM field
用PHI-Quantera XPS系统在5×109托的压力下收集XPS
emission microscope at 10 kV. XPS spectra were collected using a
光谱。
PHI Quantera XPS system under the pressure of 5×10^{-9} torr.

使用0.1 eV的步长和26 eV的通过能收集元素XPS光谱。
Elemental XPS spectra were collected using a step size of 0.1 eV and
使用284.8 eV的标准C 1s峰校准XPS光谱。
a pass energy of 26 eV. The XPS spectra were calibrated using the
使用具有Cu K辐射（=1.5406）的Rigaku D/Max
standard C 1*s* peak at 284.8 eV. XRD patterns were obtained using a
Ultima II系统获得XRD图谱。
Rigaku D/Max Ultima II system with a Cu Kα radiation (λ = 1.5406 Å).
使用TA仪器的Q-600同时TGA/DSC（差示扫描量热法），在空气中以10 °C min 1至1000 °C的加热速
TGA was conducted in air at a heating rate of 10°C min to 1000°C
率进行TGA。
using a Q-600 Simultaneous TGA/DSC (differential scanning calo-
使用红外温度计（微ε）进行温度测量，温度测量范
rimetry) from TA Instruments. The temperature measurement was
围为1000 °至3000 °C，时间分辨率为1 ms。
conducted using an infrared thermometer (Micro-Epsilon) with a temperature measurement range of 1000° to 3000°C and a time resolution
FJH期间样品的光学图像是使用超快照相机（Chronos 1.4）拍摄的。
of 1 ms. The optical image of the sample during FJH was captured
利用MATLAB将彩色图像转换为强度矩阵，
using an ultrafast camera (Chronos 1.4). The color image was con-
在此基础上拟合Stefan-Boltzmann定律得到温度图
verted into an intensity matrix using MATLAB based on which the temperature map was obtained by fitting the Stefan-Boltzmann law

$$j = \sigma T^4 \quad (1)$$

其中j是黑体辐射发射度，是一个比例常数，T是热力学温度。
where j is the blackbody radiant emittance, σ is a constant of proportionality, and T is the thermodynamic temperature.

计算
Calculation
溶解曲线根据Visual MINT-EQ 3.1计算。添加额外Cl以补偿费用余额。
The dissolution curves are calculated on the basis of Visual MINT-EQ 3.1. Extra Cl^- is added to compensate for the charge balance.
由于缺乏稀土氧化物的Ksp数据，根据相关的稀土氢氧化物估算稀土氧化物的溶解度[例如，使用
The solubility of the REE oxide is estimated on the basis of the relat-
Y(OH)3估算Y2O3的溶解]。
ed REE hydroxide [e.g., $Y(OH)_3$ was used to estimate the dissolu-
然而，氢氧化物的计
tion of Y_2O_3] due to the lack of K_{sp} data of REE oxides. Nevertheless,
算结果与之前报告中氧化物对应物的计算结果吻合良好。
the calculated results of hydroxides match well with the ones calculated from the oxide counterparts in a previous report (*7*). The sam-
特质量为1 g
的样品溶解在100 ml溶液中，以获得溶解百分比。
ples with mass of 1 g were dissolved in 100-ml solution to get the dissolution percentage.

SUPPLEMENTARY MATERIALS

Supplementary material for this article is available at https://science.org/doi/10.1126/sciadv.abm3132

REFERENCES AND NOTES

1. T. Cheisson, E. J. Schelter, Rare earth elements: Mendeleev's bane, modern marvels. *Science* **363**, 489–493 (2019).
2. J. C. K. Lee, Z. G. Wen, Pathways for greening the supply of rare earth elements in China. *Nat. Sustain.* **1**, 598–605 (2018).
3. R. K. Jyothi, T. Thenepalli, J. W. Ahn, P. K. Parhi, K. W. Chung, J.-Y. Lee, Review of rare earth elements recovery from secondary resources for clean energy technologies: Grand opportunities to create wealth from waste. *J. Clean. Prod.* **267**, 122048–122073 (2020).
4. R. K. Taggart, J. C. Hower, G. S. Dwyer, H. Hsu-Kim, Trends in the rare earth element content of U.S.-based coal combustion fly ashes. *Environ. Sci. Technol.* **50**, 5919–5926 (2016).
5. R. C. Smith, R. K. Taggart, J. C. Hower, M. R. Wiesner, H. Hsu-Kim, Selective recovery of rare earth elements from coal fly ash leachates using liquid membrane processes. *Environ. Sci. Technol.* **53**, 4490–4499 (2019).
6. W. Zhang, A. Noble, X. Yang, R. Honaker, A comprehensive review of rare earth elements recovery from coal-related materials. *Minerals* **10**, 451–478 (2020).
7. P. Liu, R. Huang, Y. Tang, Comprehensive understandings of rare earth element (REE) speciation in coal fly ashes and implication for REE extractability. *Environ. Sci. Technol.* **53**, 5369–5377 (2019).
8. P. K. Sahoo, K. Kim, M. A. Powell, S. M. Equeenuddin, Recovery of metals and other beneficial products from coal fly ash: A sustainable approach for fly ash management. *Int. J. Coal Sci. Technol.* **3**, 267–283 (2016).
9. A. Middleton, D. M. Park, Y. Jiao, H. Hsu-Kim, Major element composition controls rare earth element solubility during leaching of coal fly ash and coal by-products. *Int. J. Coal Geol.* **227**, 103532–103539 (2020).
10. E. A. Deady, E. Mouchos, K. Goodenough, B. J. Williamson, F. Wall, A review of the potential for rare-earth element resources from European red muds: Examples from Seydişehir, Turkey and Parnassus-Giona, Greece. *Mineral. Mag.* **80**, 43–61 (2016).
11. R. M. Rivera, B. Ulenaers, G. Ounoughene, K. Binnemans, T. Van Gerven, Extraction of rare earths from bauxite residue (red mud) by dry digestion followed by water leaching. *Miner. Eng.* **119**, 82–92 (2018).
12. S. Reid, J. Tam, M. F. Yang, G. Azimi, Technospheric mining of rare earth elements from bauxite residue (red mud): Process optimization, kinetic investigation, and microwave pretreatment. *Sci. Rep.* **7**, 15252 (2017).
13. S. Maroufi, R. K. Nekouei, R. Hossain, M. Assefi, V. Sahajwalla, Recovery of rare earth (i.e., La, Ce, Nd, and Pr) oxides from end-of-life Ni-MH battery via thermal isolation. *ACS Sustain. Chem. Eng.* **6**, 11811–11818 (2018).
14. V. G. Deshmane, S. Z. Islam, R. R. Bhave, Selective recovery of rare earth elements from a wide range of e-waste and process scalability of membrane solvent extraction. *Environ. Sci. Technol.* **54**, 550–558 (2020).
15. S. Peelman, D. Kooijman, J. Sietsma, Y. Yang, Hydrometallurgical recovery of rare earth elements from mine tailings and WEEE. *J. Sustain. Metall.* **4**, 367–377 (2018).
16. J. F. King, R. K. Taggart, R. C. Smith, J. C. Hower, H. Hsu-Kim, Aqueous acid and alkaline extraction of rare earth elements from coal combustion ash. *Int. J. Coal Geol.* **195**, 75–83 (2018).
17. Z. Wang, S. Dai, J. Zou, D. French, I. T. Graham, Rare earth elements and yttrium in coal ash from the Luzhou power plant in Sichuan, Southwest China: Concentration, characterization and optimized extraction. *Int. J. Coal Geol.* **203**, 1–14 (2019).
18. R. K. Taggart, J. C. Hower, H. Hsu-Kim, Effects of roasting additives and leaching parameters on the extraction of rare earth elements from coal fly ash. *Int. J. Coal Geol.* **196**, 106–114 (2018).
19. S. Dou, J. Xu, X. Cui, W. Liu, Z. Zhang, Y. Deng, W. Hu, Y. Chen, High-temperature shock enabled nanomanufacturing for energy-related applications. *Adv. Energy Mater.* **10**, 2001331–2001345 (2020).
20. Y. G. Yao, Z. N. Huang, P. F. Xie, S. D. Lacey, R. J. Jacob, H. Xie, F. J. Chen, A. M. Nie, T. C. Pu, M. Rehwoldt, D. W. Yu, M. R. Zachariah, C. Wang, R. Shahbazian-Yassar, J. Li, L. B. Hu, Carbothermal shock synthesis of high-entropy-alloy nanoparticles. *Science* **359**, 1489–1494 (2018).
21. R. Jiang, Y. Da, X. Han, Y. Chen, Y. Deng, W. Hu, Ultrafast synthesis for functional nanomaterials. *Cell Rep. Phys. Sci.* **2**, 100302 (2021).
22. Y. Chen, G. C. Egan, J. Wan, S. Zhu, R. J. Jacob, W. Zhou, J. Dai, Y. Wang, V. A. Danner, Y. Yao, K. Fu, Y. Wang, W. Bao, T. Li, M. R. Zachariah, L. Hu, Ultra-fast self-assembly and stabilization of reactive nanoparticles in reduced graphene oxide films. *Nat. Commun.* **7**, 12332 (2016).
23. C. Wang, W. Ping, Q. Bai, H. Cui, R. Hensleigh, R. Wang, A. H. Brozena, Z. Xu, J. Dai, Y. Pei, C. Zheng, G. Pastel, J. Gao, X. Wang, H. Wang, J.-C. Zhao, B. Yang, X. Zheng, J. Luo, Y. Mo, B. Dunn, L. Hu, A general method to synthesize and sinter bulk ceramics in seconds. *Science* **368**, 521–526 (2020).
24. D. X. Luong, K. V. Bets, W. A. Algozeeb, M. G. Stanford, C. Kittrell, W. Chen, R. V. Salvatierra, M. Q. Ren, E. A. McHugh, P. A. Advincula, Z. Wang, M. Bhatt, H. Guo, V. Mancevski, R. Shahsavari, B. I. Yakobson, J. M. Tour, Gram-scale bottom-up flash graphene synthesis. *Nature* **577**, 647–651 (2020).
25. W. Chen, J. T. Li, Z. Wang, W. A. Algozeeb, D. X. Luong, C. Kittrell, E. A. McHugh, P. A. Advincula, K. M. Wyss, J. L. Beckham, M. G. Stanford, B. Jiang, J. M. Tour, Ultrafast and controllable phase evolution by flash Joule heating. *ACS Nano* **15**, 11158–11167 (2021).
26. N. H. Barbhuiya, A. Kumar, A. Singh, M. K. Chandel, C. J. Arnusch, J. M. Tour, S. P. Singh, The Future of flash graphene for the sustainable management of solid waste. *ACS Nano* **15**, 15461–15470 (2021).
27. W. A. Algozeeb, P. E. Savas, D. X. Luong, W. Chen, C. Kittrell, M. Bhat, R. Shahsavari, J. M. Tour, Flash graphene from plastic waste. *ACS Nano* **14**, 15595–15604 (2020).
28. P. A. Advincula, D. X. Luong, W. Chen, S. Raghuraman, R. Shahsavari, J. M. Tour, Flash graphene from rubber waste. *Carbon* **178**, 649–656 (2021).
29. M. Y. Stuckman, C. L. Lopano, E. J. Granite, Distribution and speciation of rare earth elements in coal combustion by-products via synchrotron microscopy and spectroscopy. *Int. J. Coal Geol.* **195**, 125–138 (2018).
30. S. V. Ushakov, K. B. Helean, A. Navrotsky, L. A. Boatner, Thermochemistry of rare-earth orthophosphates. *J. Mater. Res.* **16**, 2623–2633 (2001).
31. Y. Hikichi, T. Nomura, Melting temperatures of monazite and xenotime. *J. Am. Ceram. Soc.* **70**, C-252–C-253 (1987).
32. A. Kolker, C. Scott, J. C. Hower, J. A. Vazquez, C. L. Lopano, S. F. Dai, Distribution of rare earth elements in coal combustion fly ash, determined by SHRIMP-RG ion microprobe. *Int. J. Coal Geol.* **184**, 1–10 (2017).
33. D. Smolka-Danielowska, Rare earth elements in fly ashes created during the coal burning process in certain coal-fired power plants operating in Poland - Upper Silesian Industrial Region. *J. Environ. Radioact.* **101**, 965–968 (2010).
34. S. Dai, L. Zhao, J. C. Hower, M. N. Johnston, W. Song, P. Wang, S. Zhang, Petrology, mineralogy, and chemistry of size-fractioned fly ash from the Jungar Power Plant, Inner Mongolia, China, with emphasis on the distribution of rare earth elements. *Energy Fuel* **28**, 1502–1514 (2014).
35. D. Barreca, G. A. Battiston, D. Berto, R. Gerbasi, E. Tondello, Y_2O_3 thin films characterized by XPS. *Surf. Sci. Spectra* **8**, 234–239 (2001).

36. K. M. Cole, D. W. Kirk, S. J. Thorpe, Surface Y_2O_3 layer formed on air exposed Y powder characterized by XPS. *Surf. Sci. Spectra* **27**, 024010–024020 (2020).
37. A. M. de Asha, R. M. Nix, Oxidation of lanthanum overlay ers on Cu(111). *Surf. Sci.* **322**, 41–50 (1995).
38. J. P. H. Li, X. Zhou, Y. Pang, L. Zhu, E. I. Vovk, L. Cong, A. P. van Bavel, S. Li, Y. Yang, Understanding of binding energy calibration in XPS of lanthanum oxide by in situ treatment. *Phys. Chem. Chem. Phys.* **21**, 22351–22358 (2019).
39. N. N. Greenwood, A. Earnshaw, *Chemistry of the Elements* (Butterworth-Heinemann, ed. 2, 1997), 299 pp.
40. R. F. Service, Red alert. *Science* **369**, 910–911 (2020).
41. M. OchsenkuhnPetropulu, T. Lyberopulu, K. M. Ochsenkuhn, G. Parissakis, Recovery of lanthanides and yttrium from red mud by selective leaching. *Anal. Chim. Acta* **319**, 249–254 (1996).
42. M. Boni, G. Rollinson, N. Mondillo, G. Balassone, L. Santoro, Quantitative mineralogical characterization of karst bauxite deposits in the southern Apennines, Italy. *Econ. Geol.* **108**, 813–833 (2013).
43. X. Zeng, J. A. Mathews, J. Li, Urban mining of e-waste is becoming more cost-effective than virgin mining. *Environ. Sci. Technol.* **52**, 4835–4841 (2018).
44. M. A. Alam, L. Zuga, M. G. Pecht, Economics of rare earth elements in ceramic capacitors. *Ceram. Int.* **38**, 6091–6098 (2012).
45. D. Bauer, D. Diamond, J. Li, D. Sandalow, P. Telleen, B. Wanner, *Critical Materials Strategy* (U.S. Department of Energy, 2010).
46. V. V. Seredin, S. Dai, Coal deposits as potential alternative sources for lanthanides and yttrium. *Int. J. Coal Geol.* **94**, 67–93 (2012).
47. T. Wen, Q. Zhang, C. Guo, X. Liu, L. Pang, J. Zhao, Y. Yin, W. Shi, W. Chen, X. Tan, 3-MV compact very fast transient overvoltage generator for testing ultra-high-voltage gas-insulated switchgear. *IEEE Electr. Insul. Mag.* **30**, 26–33 (2014).
48. W. Chen, X. Cui, Foreword for the special section on AC and DC ultra high voltage technologies. *CSEE J. Power Energy Syst.* **1**, 1–2 (2015).
49. S. Peelman, Z. H. I. Sun, J. Sietsma, Y. Yang, in *Rare Earths Industry,* I. Borges De Lima, W. Leal Filho, Eds. (Elsevier, 2016), pp. 319–334.
50. R. Kim, H. Cho, K. N. Han, K. Kim, M. Mun, Optimization of acid leaching of rare-earth elements from Mongolian apatite-based Ore. *Minerals* **6**, 63 (2016).
51. F. Xie, T. A. Zhang, D. Dreisinger, F. Doyle, A critical review on solvent extraction of rare earths from aqueous solutions. *Miner. Eng.* **56**, 10–28 (2014).
52. M. T. Schatzmann, M. L. Mecartney, P. E. D. Morgan, Synthesis of monoclinic monazite, $LaPO_4$, by direct precipitation. *J. Mater. Chem.* **19**, 5720–5722 (2009).
53. Current prices of rare earths; https://en.institut-seltene-erden.de/aktuelle-preise-von-seltenen-erden/.
54. W. D. Judge, G. Azimi, Recent progress in impurity removal during rare earth element processing: A review. *Hydrometallurgy* **196**, 105435–105474 (2020).
55. W. Zhang, X. Xie, X. Tong, Y. Du, Q. Song, D. Feng, Study on the effect and mechanism of impurity aluminum on the solvent extraction of rare earth elements (Nd, Pr, La) by P204-P350 in chloride solution. *Minerals* **11**, 61–73 (2021).
56. Q. Ye, G. Li, B. Deng, J. Luo, M. Rao, Z. Peng, Y. Zhang, T. Jiang, Solvent extraction behavior of metal ions and selective separation Sc^{3+} in phosphoric acid medium using P204. *Sep. Purif. Technol.* **209**, 175–181 (2019).
57. R. G. Silva, C. A. Morais, E. D. Oliveira, Selective precipitation of rare earth from non-purified and purified sulfate liquors using sodium sulfate and disodium hydrogen phosphate. *Miner. Eng.* **134**, 402–416 (2019).
58. F. Li, A. Gong, L. Qiu, W. Zhang, J. Li, Z. Liu, Diglycolamide-grafted Fe_3O_4/polydopamine nanomaterial as a novel magnetic adsorbent for preconcentration of rare earth elements in water samples prior to inductively coupled plasma optical emission spectrometry determination. *Chem. Eng. J.* **361**, 1098–1109 (2019).
59. Z. Lou, X. Xiao, M. Huang, Y. Wang, Z. Xing, Y. Xiong, Acrylic acid-functionalized metal–organic frameworks for Sc(III) selective adsorption. *ACS Appl. Mater. Inter.* **11**, 11772–11781 (2019).
60. C. Brabant, A. Khodakov, A. Griboval-Constant, Promotion of lanthanum-supported cobalt-based catalysts for the Fischer-Tropsch reaction. *C. R. Chim.* **20**, 40–46 (2017).
61. L. Schlapbach, H. R. Scherrer, XPS core level and valence band spectra of LaH_3. *Solid State Commun.* **41**, 893–897 (1982).
62. A. Shelyug, A. Mesbah, S. Szenknect, N. Clavier, N. Dacheux, A. Navrotsky, Thermodynamics and stability of rhabdophanes, hydrated rare earth phosphates $REPO_4 \cdot n\ H_2O$. *Front. Chem.* **6**, 604 (2018).
63. D. R. Lide, *CRC Handbook of Chemistry and Physics* (CRC Press, 2005); www.hbcpnetbase.com.
64. D. D. Wagman, W. H. Evans, V. B. Schumm, I. Halow, *The NBS Tables of Chemical Thermodynamic Properties. Selected Values for Inorganic and C1 and C2 Organic Substances in SI Units* (American Chemical Society, 1982).
65. Y. Zhang, I.-H. Jung, Critical evaluation of thermodynamic properties of rare earth sesquioxides (RE = La, Ce, Pr, Nd, Pm, Sm, Eu, Gd, Tb, Dy, Ho, Er, Tm, Yb, Lu, Sc and Y). *Calphad* **58**, 169–203 (2017).
66. S. A. Wood, I. M. Samson, The aqueous geochemistry of gallium, germanium, indium and scandium. *Ore Geol. Rev.* **28**, 57–102 (2006).
67. Z. S. Cetiner, S. A. Wood, C. H. Gammons, The aqueous geochemistry of the rare earth elements. Part XIV. The solubility of rare earth element phosphates from 23 to 150 degrees C. *Chem. Geol.* **217**, 147–169 (2005).

Acknowledgments: We thank H. H.-Kim from Duke University for providing the CFA samples and E. Balomenos from MYTILINEOS for providing the BR samples and helpful discussion on the BR-related content in the manuscript. We acknowledge B. Chen from Rice University for helpful input with the XPS results and C. Pennington for assistance in ICP measurement. The characterization equipment used in this project is, in part, from the Shared Equipment Authority (SEA) at Rice University. **Funding:** The funding of the research is provided by Air Force Office of Scientific Research (FA9550-19-1-0296), U.S. Army Corps of Engineers, ERDC (W912HZ-21-2-0050), and the Department of Energy (DE-FE0031794). **Author contributions:** B.D. and J.M.T. conceived the idea to use FJH to obtain REE from waste. B.D. conducted most of the experimental works with the help of R.A.C. and Z.W. D.X.L. designed the FJH system. X.W. and M.B.T. conducted the calculation on the REE species solubility. B.D. and J.M.T. wrote the manuscript. All aspects of the research were overseen by J.M.T. All authors discussed the results and commented on the manuscript. **Competing interests:** Rice University owns the intellectual property (IP) on the REE recovery from secondary wastes including CFA, BR, and e-waste by the FJH process. A patent application on the process for REE recovery has been filed by Rice University, but to date, that IP has not been licensed. Universal Matter Inc. has been mentioned as a company that is scaling up the FJH process for graphene production, and their equipment might be leveraged for scaling the FJH process for REE isolation. Universal Matter Inc. has licensed their graphene production technology from Rice University. J.M.T. is a stockholder in Universal Matter Inc., although he is not an officer, director, or employee of that company. Conflicts of interest are mitigated through regular disclosure to and compliance with the Rice University Office of Sponsored Programs and Research Compliance. The authors declare that they have no other competing interests. **Data and materials availability:** All data needed to evaluate the conclusions in the paper are present in the paper and/or the Supplementary Materials.

Submitted 8 September 2021
Accepted 15 December 2021
Published 9 February 2022
10.1126/sciadv.abm3132

Science Advances

Rare earth elements from waste

Bing DengXin WangDuy Xuan LuongRobert A. CarterZhe WangMason B. TomsonJames M. Tour

Sci. Adv., 8 (6), eabm3132.

Science Advances (ISSN) is published by the American Association for the Advancement of Science. 1200 New York Avenue NW, Washington, DC 20005. The title *Science Advances* is a registered trademark of AAAS.